Multi-Objective Engineering of Fibrin-Selective Thrombolytic Proteases with Enhanced Biocatalytic Efficiency and Inhibition Resistance

Toul M.[1,2,#], Slonkova V.[1,#], Mican J.[1,2,#], Thalerova S.[2,3], Peskova M.[2,3,4], Kittova P.[2,4,5], Scheer P.[2,6], Hlozkova J.[2,6], Brhelova E.[2,7], Aksu D.A.[2,6], Biskupic J.[2,7], Kuchynka M.[2,7], Ondrus J.[2,8], Kasparek P.[9], Batkova T.[2,9,10], Marek M.[1,2], Vitecek J.[2,3], Kubala L.[2,3], Mikulik R.[2,10], Damborsky J.[1,2], Bednar D.[1,2,*], Prokop Z.[1,2,*]

1. Loschmidt Laboratories, Department of Experimental Biology and RECETOX, Faculty of Science, Masaryk University, Kamenice 5/C13, 625 00 Brno, Czech Republic
2. International Clinical Research Center, St. Anne's University Hospital, Pekarska 53, 656 91 Brno, Czech Republic
3. Department of Biophysics of Immune System, Institute of Biophysics of the Czech Academy of Sciences, Kralovopolska 135, 612 65 Brno, Czech Republic
4. Department of Biochemistry, Faculty of Science, Masaryk University, Kamenice 5, 625 00 Brno, Czech Republic
5. Department of Biochemistry, Faculty of Medicine, Masaryk University, Kamenice 5, 625 00 Brno, Czech Republic
6. Department of Pharmacology and Toxicology, Faculty of Pharmacy, Masaryk University, Palackeho trida 1946/1, 612 00 Brno, Czech Republic
7. Department of Chemical Drugs, Faculty of Pharmacy, Masaryk University, Palackeho trida 1946/1, 612 00 Brno, Czech Republic
8. Veterinary Research Institute, Hudcova 296/70, 621 00 Brno, Czech Republic
9. BioVendor LM, Karasek 1767/1, 621 00 Brno, Czech Republic
10. Department of Neurology, Tomas Bata Regional Hospital, Havlickovo nabrezi 600, 762 75 Zlin, Czech Republic

[#] These authors contributed equally to the work

* Corresponding authors

Abstract

Thrombolytic enzymes represent an important class of proteolytic biocatalysts for medical applications, yet currently used FDA-approved variants, including alteplase and tenecteplase, remain limited by suboptimal catalytic efficiency, off-target activity, and susceptibility to inhibition. These limitations reflect the complexity of enzyme function in physiological environments, where therapeutic performance depends on the simultaneous optimization of multiple catalytic and biophysical properties. Here, we introduce a multi-objective enzyme engineering strategy for the design of next-generation thrombolytic proteases, explicitly targeting multiple properties required for therapeutic performance. Our approach combines computer-aided design, evolutionary reconstruction, and literature-guided mutation selection to improve catalytic activity, fibrin selectivity, inhibition resistance, and functional lifetime within a single workflow. This framework is coupled with systematic biochemical characterization, *in vitro* evaluation of clot penetration and fibrinolytic activity, and *in vivo* validation of efficacy and safety. By addressing multiple performance parameters simultaneously, this strategy enables efficient navigation of trade-offs that typically limit enzyme optimization. Using this approach, we identify Brnoteplase as a lead variant with enhanced fibrin selectivity, improved resistance to inhibition, and superior clot penetration, resulting in increased effective catalytic lifetime and enabling bolus administration. *In vivo* studies demonstrate enhanced thrombolysis and recanalization with reduced hemorrhagic complications. These findings provide a broadly applicable framework for designing proteolytic biocatalysts suitable for complex biological environments.

Introduction

Cardiovascular diseases, including ischemic stroke, remain the leading cause of morbidity and mortality worldwide, with a steadily increasing global burden[1]. Although mechanical thrombectomy has significantly improved outcomes in selected patients, its use is inherently limited by the need for specialized infrastructure and narrow treatment windows[2]. In contrast, enzyme-mediated thrombolysis is widely accessible, cost-effective, and straightforward to administer, making it the primary therapeutic option on a global scale[3]. However, currently available thrombolytic enzymes exhibit substantial limitations[4], underscoring the need for engineering next-generation biocatalysts with improved efficiency and safety profiles[5].

For nearly three decades, alteplase was the only U.S. Food and Drug Administration (FDA)-approved thrombolytic for acute ischemic stroke. Despite its clinical utility, alteplase shows modest recanalization rates (<50%), a short biological half-life, and an elevated risk of intracranial hemorrhage[6,7]. The recent FDA approval of tenecteplase in March 2025 introduced a second drug for acute ischemic stroke treatment[8]. As an engineered variant of alteplase, tenecteplase exhibits improved fibrin specificity and improved inhibition resistance, resulting in an extended half-life that enables bolus administration[9]. However, tenecteplase does not show clear superiority over alteplase in terms of efficacy or safety[10-13], highlighting persistent limitations of current thrombolytic enzymes.

From a catalytic perspective, thrombolytic performance arises from the interplay of multiple enzyme properties. An ideal thrombolytic enzyme should combine high catalytic efficiency toward fibrin-bound plasminogen with strict substrate selectivity and reduced binding to receptors such as the low-density lipoprotein receptor-related protein 1 (LRP1) and the N-methyl-D-aspartate receptor (NMDAR)[14]. A combination of these properties would make the 69 thrombolytic safer by decreasing hemorrhagic and neurotoxicity risks[15,16]. In parallel, enhanced resistance to plasminogen activator inhibitor-1 (PAI-1) prolongs the biological half-life, thereby increasing overall efficacy throughout the therapeutic window and enabling convenient bolus administration[17]. These requirements define a multidimensional optimization problem in which improving a single parameter is insufficient to achieve overall therapeutic performance.

73 Here, we introduce a multi-objective enzyme engineering strategy to develop next-
74 generation thrombolytic proteases with enhanced biocatalytic and therapeutic properties
75 (**Figure 1**). The workflow integrates complementary design principles, including computer-aided
76 mutagenesis to modulate receptor interactions, literature-guided combination of beneficial
77 mutations, ancestral sequence reconstruction to access robust sequence variants, and sequence
78 database mining to identify novel functional scaffolds. These design strategies are combined with
79 systematic biochemical profiling, and hierarchical functional screening to efficiently navigate
80 sequence space while minimizing reliance on resource-intensive *in vivo* testing.

81 Using this approach, we engineered variants of plasminogen activators and identified a lead
82 candidate, Brnoteplase, with enhanced fibrin selectivity, resistance to inhibition, and improved
83 clot penetration. These improvements translate into prolonged effective catalytic lifetime and
84 improved thrombolytic performance, positioning Brnoteplase as a promising candidate for further
85 development. Beyond this specific case, our results establish a generalizable framework for the
86 multi-objective engineering of proteolytic biocatalysts operating in complex biological
87 environments, laying a foundation for the development of next-generation enzyme-based
88 therapeutics.

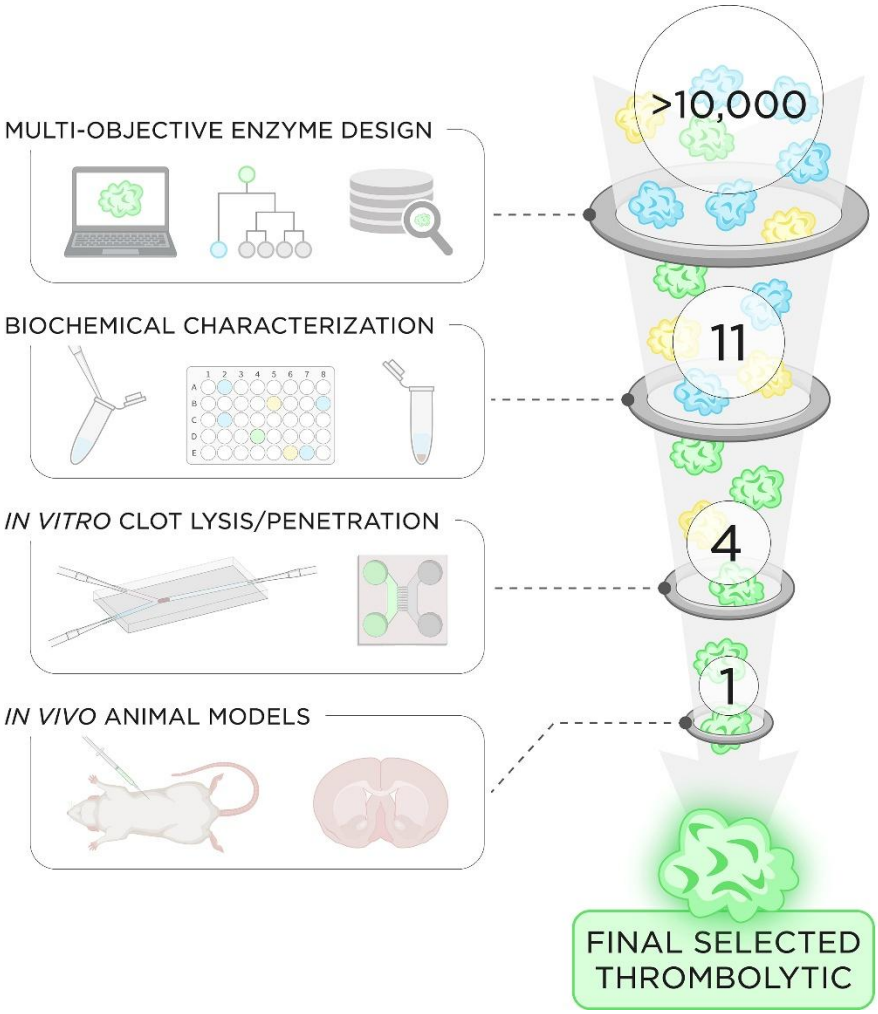

Figure 1: Multi-objective engineering workflow for the development of thrombolytic proteases. The pipeline involves (i) *in silico* rational design of new thrombolytic protein sequences, (ii) their biochemical characterization, (iii) testing in *in vitro* thrombolysis and penetration assays, and (iv) validation in *in vivo* animal rat models. The numbers in the circles correspond to the number of thrombolytic protein variants advanced to each step (grey rings) of the workflow, enabling initial screening of more than 10,000 variants and their comprehensive filtering down to a single selected thrombolytic variant for verification in resource-intensive preclinical *in vivo* models.

Methods

Computer-aided selection of mutations alleviating binding of tPA to LRP1

Computational design of alteplase variants with reduced binding to the LRP1 receptor was performed using (i) structure-based and (ii) sequence-based strategies.

In the structure-based strategy, we performed conservation and correlation analysis of lysine residues on the first four domains of alteplase, which are responsible for LRP1 binding, using the HotSpot Wizard web server[18]. Afterwards, we docked the structure of LRP1 complement-like binding repeat to tissue-type plasminogen activator (tPA) using ClusPro and RosettaDock[19]. We

105 clustered the docked structures and evaluated distances of conserved and exposed lysines of tPA
106 to the lysine-binding site of LRP1. Lastly, we have performed molecular dynamics (MD) of tPA
107 and evaluated which pairs of lysines are in the required distance of 21 to 29 Å for binding LRP1[20].
108 We designed mutant tPAs lacking specific lysines. These lysines fulfil the following criteria: (i)
109 conserved in homologous sequences, (ii) exposed on the protein surface, (iii) located on the first
110 four domains of tPA responsible for LRP1 binding, (iv) located on the interface with LRP1
111 complement-binding repeat in cluster centres of docked structures, and (v) being within 21 – 29
112 Å of another lysine residue in tPA during MD simulations.

113 In the sequence-based strategy, we compared the tPA sequence to its homolog, desmoteplase,
114 which competitively binds LRP1[21]. In the pairwise sequence alignment, we identified lysines in
115 both tPA and desmoteplase at homologous positions. These lysines are likely candidates to
116 mediate LRP1 binding.

117 Lysine positions identified by structure- and sequence-based strategies were subjected to *in*
118 *silico* saturation mutagenesis using the Rosetta ddg_monomer application. Mutated residues that
119 retained thermodynamical stability were selected for experimental characterization.

120 **Combining beneficial tPA mutations from literature:**

121 To identify mutations for enhancing the efficacy and safety of tPA, we performed
122 a comprehensive literature review on the structural biology and protein engineering
123 of thrombolytics. We then sought an innovative combination of mutations to improve tPA efficacy
124 and safety and combined them into a multiple mutant.

125 **Ancestral sequence reconstruction of tPA-related proteins**

126 The sequence of tPA, including the signal peptide, was submitted to the FireProt^{ASR} web server[22].
127 The calculation was performed using default settings. Ancestral sequences for experimental
128 characterization were selected using the following criteria: (i) as few insertions or deletions
129 compared to tPA as possible, (ii) preserved catalytic residues, and (iii) preserved functionally
130 important residues known to influence different tPA functions.

131 **Mining novel enzymes from sequence databases**

132 EnzymeMiner was used to search for novel thrombolytic enzymes in protein sequence
133 databases[23]. Two separate runs were performed using tPA and desmoteplase as query sequences.
134 Proteins with transmembrane regions or mutated catalytic residues were discarded. Moreover,
135 proteins had to contain key domains for plasminogen activation and fibrin binding and score a
136 predicted solubility higher than the query sequence. After filtering for these characteristics,
137 proteins with interesting properties were selected manually.

138 **Construction of mutant gene sequences**

139 For each designed thrombolytic variant, a synthetic gene (Genscript) was cloned into the
140 expression vector pcDNA3.1 (Thermo Fisher Scientific). *E. coli* strain TOP10F (Thermo Fisher
141 Scientific) was transformed with the plasmid construct. Plasmid DNA was isolated for transient
142 transfection using Plasmid Giga Kit (Qiagen).

143 **Heterologous gene expression and protein isolation**

144 HEK-293E cells (ATCC® CRL-10852™) were adapted to suspension growth in HyClone™
145 CDM4HEK293 serum-free medium (Cytiva) supplemented with 4 mM L-glutamine (AppliChem).
146 Prior to transient transfection, HEK-293E cells were centrifuged at 250 g for 10 minutes and
147 resuspended at the density of $2x10^7$ cells/ml in the Gibco™ FreeStyle™ 293 expression medium
148 (Thermo Fisher Scientific). HEK-293E cells were transiently transfected by plasmid DNA and linear
149 25-kDa polyethyleneimine (Polysciences) at a 1:2 ratio and a final concentration of 25 and 50
150 ug/mL, respectively. Plasmid pmaxGFP at 5 % of the total DNA content was added as a positive
151 control of the transfection process. Four hours after transfection, cells were diluted with HyClone
152 medium containing 2 mM L-glutamine. The cells were cultured at 37 °C and 130 rpm in an
153 incubator shaker (New Brunswick Innova® 44/44R). The culture supernatants were harvested 7
154 days post-transfection. The supernatant was purified on Ni-NTA column (Protino, Macherey-
155 Nagel) connected to the BioLogic DuoFlow FPLC system (Bio-Rad) and equilibrated with the
156 purification buffer (10 mM Tris-HCl pH 7.5, 200 mM NaCl). The thrombolytic protein bound to the
157 column was washed and eluted with 10 mM and 250 mM imidazole in buffer 10 mM Tris-HCl buffer

158 pH 7.5 with 200 mM NaCl and 200 mM L-Arginine. Subsequently, the protein was purified on the
159 Superose 6 SEC column (GE Healthcare) equilibrated with PBS buffer pH 7.4, 200 mM L-Arginine.
160 The protein was supplemented with 0.01 % of Tween 80 and stored at +4 °C.

161 **Protein thermostability measurement**

162 Protein thermostability was determined by analyzing changes in protein intrinsic tryptophan
163 fluorescence with increasing temperature using the nanoscale differential scanning fluorimetry
164 (nanoDSF) instrument Prometheus NT.48 (NanoTemper Technologies). Each measurement was
165 performed in triplicate in phosphate-buffered saline PBS pH 7.4 (10 mM Na_2HPO_4, 1.8 mM KH_2PO_4,
166 2.7 mM KCl, 137 mM NaCl) containing 3.5 % L-arginine, and 0.01 % Tween 80. The fluorescence
167 was monitored at temperatures ranging from 20 °C to 100 °C with a temperature ramp of 1
168 $°C.min^{-1}$ and the values of the fluorescence ratio at 350/330 nm were plotted against
169 temperature. The values of onset temperature (T_{onset}) and melting temperature (T_m) were
170 determined using the manufacturer-provided software after deriving the obtained fluorescence
171 curves. The final values were expressed as averages of individual replicates and their respective
172 standard deviations.

173 **Determination of enzymatic activity and fibrin(ogen) stimulation and selectivity**

174 The activities of thrombolytic enzymes were measured using the fluorogenic substrate D-VLK-
175 AMC (AAT Bioquest), which is converted by the generated plasmin molecules to the fluorescent
176 product 7-amino-4-methylcoumarin (AMC), whose fluorescence was monitored based on the
177 previously published protocol[24]. All the experiments were performed at 37 °C in phosphate-
178 buffered saline PBS pH 7.4 (10 mM Na_2HPO_4, 1.8 mM KH_2PO_4, 2.7 mM KCl, 137 mM NaCl) containing
179 1 mM $CaCl_2$, 0.0035 % L-arginine, and 0.01 % Tween 80 and each measurement was repeated in
180 three replicates. The activities were determined in the absence but also in the presence of
181 fibrinogen or fibrin that served as stimulation agents. In the case of fibrin stimulation, small
182 fibrin clots were formed in a microplate well of a black clear bottom 96-well plate by mixing 8
183 µL of human fibrinogen (HYPHEN BioMed) with 2 µL of human thrombin (Sigma-Aldrich). The wells
184 were sealed with an adhesive foil to prevent evaporation and kept at room temperature for an

185 hour to ensure complete polymerization and clot formation. In the case of fibrinogen stimulation,
186 the microplate wells were filled with 8 μL of human fibrinogen mixed with 2 μL of the reaction
187 buffer only. In the absence of any stimulant, only 10 μL of the reaction buffer was injected. After
188 that, all the microplate wells were added 50 μL of human plasminogen (Roche Diagnostics), 30
189 μL of D-VLK-AMC, and 10 μL of the tested thrombolytic to initiate the reaction. The resulting
190 concentrations in microplate wells were 3.0 μM fibrin (where applicable), 0.04 UN/mL thrombin
191 (where applicable), 3.0 μM fibrinogen (where applicable), 4.5 μM plasminogen, 200 μM D-VLK-
192 AMC, and 0.08 nM tested thrombolytic. The microplate containing all the tested conditions was
193 then sealed with a transparent adhesive foil and the enzymatic activity was measured by
194 monitoring the increase in fluorescence with time using the microplate reader FLUOstar OPTIMA
195 (BMG Labtech). The emission was detected every 60 seconds at 460 nm upon excitation at 360
196 nm with the instrument gain set to 1,100 and the bottom reading position.

197 **Activity and stimulation kinetic data analysis**

198 All the curves of increasing AMC fluorescence with time were first recalculated to AMC
199 concentration changes with time based on the calibration curve that was obtained by measuring
200 fluorescence of various increasing concentrations of the AMC standard (Sigma-Aldrich) ranging
201 from 0 to 1000 μM. The concentration dependence exhibited an exponential trend, so the
202 calibration curve was constructed by fitting the calibration points with the exponential **Equation**
203 **1** to obtain the calibration factors F_a, F_b, and F_c.

$$\text{Fluorescence} = F_a \cdot (1 - e^{-F_b \cdot [\text{AMC}]}) + F_c \quad (1)$$

204 Due to the coupled nature of the applied assay, the initial phase of each recalculated kinetic
205 curve was fitted with the quadratic **Equation 2**, where v_0 corresponds to the determined initial
206 rate of the enzymatic reaction, t_0 to the dead-time between the manual mixing of the assay
207 components and the start of the measurement, and c to the initial y-axis offset. Final values of
208 initial rates (activities) were expressed as average ± standard deviation for each measured
209 sample and condition.

$$[AMC] = v_0 \cdot (t + t_0)^2 + c \quad (2)$$

210 Stimulation factors and selectivities were determined according to the previously postulated
211 definitions[25]. Stimulation factor for the fibrinogen stimulation ($Stim_{FG}$) or the fibrin stimulation
212 ($Stim_{FN}$) was calculated as a ratio of the activity in the presence of the stimulant ($v_{0,FG}$ or $v_{0,FN}$)
213 over the activity in the absence of the stimulant (v_0), as summarized in **Equation 3 and 4**.
214 Selectivity (Sel_{FN}) towards fibrin (with respect to fibrinogen) was then calculated as a ratio of
215 stimulation factors in the presence of fibrin over fibrinogen according to **Equation 5**. The
216 resulting value was relativized to alteplase and statistically compared using two-sample *t*-test.

$$Stim_{FG} = \frac{v_{0,FG}}{v_0} \quad (3)$$

$$Stim_{FN} = \frac{v_{0,FN}}{v_0} \quad (4)$$

$$Sel_{FN} = \frac{Stim_{FN}}{Stim_{FG}} = \frac{v_{0,FN}}{v_{0,FG}} \quad (5)$$

217 **Plasminogen activator inhibitor 1 (PAI-1) inhibition resistance**

218 The potency of thrombolytic inhibition was analyzed by determining the fraction of active
219 thrombolytics at different PAI-1 concentrations based on the previously published protocol[24]. The
220 experiment was performed at 37 °C in phosphate-buffered saline PBS pH 7.4 (10 mM Na_2HPO_4,
221 1.8 mM KH_2PO_4, 2.7 mM KCl, 137 mM NaCl) containing 1 mM $CaCl_2$, 0.0035 % L-arginine, and 0.01
222 % Tween 80, and each measurement was repeated in three replicates. 40 µL of PAI-1 (Sigma-
223 Aldrich) was mixed with 10 µL of a tested thrombolytic and the sealed mixture was incubated at
224 37 °C for 60 min while shaking at 180 rpm to ensure that the interaction with PAI-1 reached
225 equilibrium. The resulting concentrations in the inhibition mixture were 0–1.5 µM PAI-1 and 0.16
226 µM thrombolytic. Residual activity was determined by transferring 10 µL of the inhibition mixture
227 into a microplate well of a black clear bottomed 96-well plate and mixing it with 40 µL of the
228 tPA fluorogenic substrate Boc-L-(p-F)FPR-ANSN-H-C_2H_5 (US Biological) to initiate the enzymatic
229 reaction. The resulting fluorogenic substrate concentration was 200 µM. The microplate was
230 sealed with a transparent adhesive foil and the enzymatic activity was detected by monitoring

231 the increase in fluorescence over time using the microplate reader FLUOstar Omega (BMG
232 Labtech). The emission was detected every 60 seconds at 460 nm upon excitation at 360 nm with
233 the instrument gain set to 580 and the bottom reading position.

234 **Inhibition resistance data analysis**

235 The linear phase of each fluorescence kinetic curve was fitted with the linear **Equation 6** where
236 the slope v_i corresponds to the rate of the inhibited enzymatic reaction (residual activity) and F_0
237 to the initial fluorescence offset. Since the fluorogenic substrate was converted directly by the
238 tested thrombolytic enzymes with no reaction coupling and since the fluorescence of the
239 generated product was directly proportional to its concentration, fluorescence curves could be
240 fitted directly with the linear equation to reliably obtain relative values of initial rates without
241 a need for recalculation to concentration changes. Final values of initial rates were expressed as
242 average ± standard deviation for each measured sample and condition.

$$\text{Fluorescence} = v_i \cdot t + F_0 \tag{6}$$

243 Concentration dependence of determined residual activities v_i with increasing PAI-1
244 concentration was fit with **Equation 7** for a tightly bound inhibitor where c_I corresponds to the
245 total concentration of PAI-1, c_E to the total concentration of a thrombolytic enzyme, v_i to the
246 residual activity at a given concentration c_I of PAI-1, v_0 to the non-inhibited activity in the
247 absence of PAI-1, and IC_{50} to the concentration of PAI-1 causing 50 % inhibition of a tested
248 thrombolytic. The values of IC_{50} were determined for each tested thrombolytic, relativized to
249 the value for alteplase, and statistically compared using a two-sample *t*-test.

$$c_I = c_E \cdot \left(1 - \frac{v_i}{v_0}\right) + \left(IC_{50} - \frac{c_E}{2}\right) \cdot \left(\frac{v_0}{v_i} - 1\right) \tag{7}$$

250 **Fibrin binding and affinity**

251 Affinities of thrombolytics towards fibrin were analyzed by indirectly determining the level of
252 fibrin-bound thrombolytics at various fibrin concentrations based on the previously published
253 protocol[24]. The experiment was performed at 37 °C in phosphate-buffed saline PBS pH 7.4 (10
254 mM Na_2HPO_4, 1.8 mM KH_2PO_4, 2.7 mM KCl, 137 mM NaCl) containing 1 mM $CaCl_2$, 0.0035 % L-

255 arginine, and 0.01 % Tween 80 and each measurement was repeated in three replicates. 320 μL
256 of plasminogen-free human fibrinogen (HYPHEN BioMed) was premixed with 40 μL of a tested
257 thrombolytic and the clotting was initiated by the addition of 40 μL of human thrombin (Sigma-
258 Aldrich). The resulting concentrations in the polymerization mixture were 0–38 μM fibrinogen, 16
259 nM (alteplase, Alt01, Alt02, Alt03, AltAnc02, AltEM03, DesEM01) or 235 nM (tenecteplase,
260 Brnoteplase, DesEM02, desmoteplase) thrombolytic, and 2 UN/mL thrombin. This mixture was
261 incubated at 37 °C for 60 min while shaking at 180 rpm to ensure that a complete clot formation
262 was achieved. The clots with bound thrombolytics were separated by centrifugation at 4 °C and
263 15,000 rpm for 30 minutes and the amount of unbound thrombolytic in the supernatant was
264 determined by residual activity measurement. 20 μL of the supernatant was carefully transferred
265 into a microplate well of a black clear bottom 96-well plate and mixed with 50 μL of human
266 plasminogen (Roche Diagnostics) and 30 μL of the fluorogenic substrate D-VLK-AMC (AAT
267 Bioquest) to initiate the enzymatic reaction. The resulting concentrations in a microplate well
268 were 2.3 μM plasminogen and 200 μM D-VLK-AMC. The microplate was sealed with a transparent
269 adhesive foil and the enzymatic activity was detected by monitoring an increase of fluorescence
270 with time using the microplate reader FLUOstar OPTIMA (BMG Labtech). The emission was
271 detected every 60 seconds at 460 nm upon excitation at 360 nm with the instrument gain set to
272 1,100 and the bottom reading position.

273 **Fibrin binding equilibrium data analysis**

274 The values of residual plasminogen activation initial rates (activities) $v_{0,res}$, corresponding to the
275 relative amount of an unbound thrombolytic agent, were determined by fitting the kinetic curves
276 as described above in the corresponding 'Activity and stimulation kinetic data analysis' section.
277 These values were then relativized to the initial rate in the absence of fibrin ($v_{0,abs}$) according to
278 **Equation 8** in order to obtain a fraction of bound plasminogen activator (*Bind*) at a given
279 concentration of fibrin. Concentration dependence of the determined bound fraction *Bind* with
280 increasing fibrin concentration was fit with the hyperbolic **Equation 9** to obtain the value of
281 dissociation constant K_d and the percentage of the maximal fibrin binding $Bind_{lim}$. The values

282 were determined for each tested thrombolytic, relativized to the value for alteplase, and
283 statistically compared using a two-sample *t*-test.

$$\text{Bind} = \frac{v_{0,\text{abs}} - v_{0,\text{res}}}{v_{0,\text{abs}}} \cdot 100\ \% \tag{8}$$

$$\text{Bind} = \frac{Bind_{\text{lim}} \cdot [\text{fibrin}]}{K_{\text{d}} + [\text{fibrin}]} \tag{9}$$

284 **Preparation of clots and fibrin gel for *in vitro* assays**

285 Semi-synthetic clots were prepared by mixing human fibrinogen (Tisseel Lyo kit, Baxter, dissolved
286 in water for injection to reach the concentration of 52 mg/mL), human thrombin (Tisseel Lyo
287 kit, Baxter, dissolved in 40 μM $CaCl_2$ solution to the concentration of 3.3 IU/mL), and red blood
288 cells (RBCs) isolated from healthy donors' blood in the volume ratio of 1:1:1. The incubation and
289 clotting were performed in plastic Eppendorf tubes (0.5 mL for static model; 0.2 mL for flow
290 model) for 30 min at 37 °C and >90 % relative humidity under static conditions. The prepared
291 clots were immediately introduced into the model. The final concentrations of components in
292 the prepared clots were 17.3 mg/mL fibrinogen, 1.1 IU/mL thrombin, and $4.2 \cdot 10^9$ RBCs/mL and
293 the total clot volume was 90 μL for the static model and 60 μL for the flow model.

294 RBC dominant clots were prepared from 200 μL of healthy donors' whole blood without
295 anticoagulant by clotting in borax glass tubes (inner diameter 8 mm) for 3.5 h at 37 °C and >90
296 % relative humidity under static conditions. The prepared clots were immediately introduced
297 into the model.

298 Fibrin gel was prepared from the mixture of fibrinogen (Tisseel Lyo kit, Baxter, dissolved in water
299 for injection to the concentration of 34.6 mg/mL) and thrombin (Tisseel Lyo kit, Baxter, dissolved
300 in 40 μM $CaCl_2$ solution to the concentration of 2.2 IU/mL) in the volume ratio of 1:1. The
301 incubation and the clotting was performed inside micro-slide channels for 30 min at 37 °C and
302 >90 % relative humidity under static conditions. The final concentrations of the components in
303 the prepared fibrin gel were 17.3 mg/mL fibrinogen and 1.1 IU/mL thrombin and the total volume
304 per micro-slide channel was 30 μL.

305 All blood donors had agreed to donate blood samples on the premise of signed informed consent
306 for the collection of blood. Individuals, who had received acetylsalicylic acid, non-steroidal anti-
307 inflammatory, or antiplatelet drugs within 7 days before blood collection, were excluded.

308 ***In vitro* thrombolytic models**

309 Thrombolytic experiments were performed in static and flow *in vitro* models that were described
310 in contemporary literature[26,27] but were optimized to determine the suitably measurable effect
311 of alteplase in a highly reproducible manner, as reported in previous publications[28–31]. Briefly,
312 the static model consisted of 1.5 mL plastic Eppendorf tubes filled with fresh frozen human
313 plasma (177RM, Monobind Inc.) medium to a total volume of 500 µL, in which the clots were
314 individually incubated. The tubes were incubated at 37 °C in a dry-block incubator for 60 minutes
315 (the same amount of time as indicated for alteplase treatment of stroke patients).

316 The flow model consisted of silicone chips made of Sylgard 184 Silicone Elastomer (Dow Corning),
317 which were prepared according to human middle cerebral artery anatomy, with narrowings
318 dimensionally based on patient CT scans (n = 4). The bifurcation was included to enable
319 permanent circulation in the system. Each silicone chip was connected by plastic pipes (internal
320 diameter 3.1 mm) to the 8-channel pump head peristaltic pump MINIPULS 3 (Gilson Inc.), and
321 the entire system was maintained at 37 °C for incubation lasting 180 min. This arrangement
322 maintained the hydrodynamic forces involved in clot removal[32], whereby a pressure gradient of
323 10 mm Hg was generated across the occlusion.

324 Both semi-synthetic and red blood cell dominant clots (preparation described in the
325 corresponding 'Preparation of clots and fibrin gel for in vitro assays' section above) were
326 separately employed in both thrombolytic models and the thrombolytic efficiencies were
327 compared. The final concentrations of tested thrombolytic enzymes were selected to be
328 consistent with the clinically relevant dosage indicated for patients with ischemic stroke (1.3
329 µg/mL), according to the manufacturer's instructions and supporting pharmacokinetic data[33].
330 Alternatively, 10-fold lower and 2-, 5-, 10-, and 50-fold higher concentrations were tested as
331 well.

332 ***In vitro* lytic efficacy analysis**

333 Clot lysis in the static model was determined by measuring clot mass loss[27–29,31,34] and by
334 spectrophotometric determination of RBC release into the incubation medium at 575 nm[28,29,31].
335 Clot lysis in the flow model was determined by measuring recanalization time, clot length
336 changes, and spectrophotometric determination of RBC release[28,30,31]. Recanalization frequency
337 was determined as a percentage ratio of complete recanalization to the total number of samples
338 in the respective treatment group. Relative clot reduction was determined as a percentage of
339 clot area reduction prior to clot release from the narrowed occlusion site. In addition, the
340 thrombolysis rate was calculated using linear regression of relative clot reduction at 10-minute
341 intervals. Data were expressed as mean ± standard deviation, if not otherwise indicated. The
342 generated box plots were presented as mean value (cross), median (line), interquartile range
343 (box), and minimum and maximum value (whiskers). ANOVA with post-hoc Tukey's HSD test was
344 used to compare data. P-values ≤ 0.05 were considered to be statistically significant. All analyses
345 were performed using GraphPad Prism (GraphPad Software Inc.).

346 ***In vitro* penetration microarray**

347 Penetration experiments were performed in the microarray model outlined in recent literature[35–
348 39] and optimized to provide a suitably measurable effect of alteplase in a highly repeatable
349 manner. The microarray consisted of the microslide µ-Slide VI 0.4 (Ibidi GmbH) containing
350 channels that were filled with a prepared fibrin gel (procedure described in the corresponding
351 'Preparation of clots and fibrin gel for in vitro assays' section above). Fluorescently labelled
352 plasminogen activators or bovine serum albumin (A9418, Sigma-Aldrich), as a relevant fibrin non-
353 interacting control, were applied to individual microslide channels and fluorescence intensities
354 were continuously recorded in 5 min intervals for 180 min, at 0.25 mm distance intervals up to
355 1.00 mm from the application site. The fluorescence signal was recorded using the microscope
356 ZEISS Axio Observer Z1 (Carl Zeiss AG) equipped with the metal halide fluorescence light source
357 HXP 120 (Carl Zeiss AG) and the high efficiency Filter Set 43 HE (Carl Zeiss AG). The detection
358 settings were as follows: excitation BP 550/25; beam splitter FT 570; emission BP 605/70.
359 Thrombolytic proteins and bovine serum albumin control were fluorescently labelled with

360 rhodamine B isothiocyanate (283924, Sigma-Aldrich) prior to the penetration assay according to
361 the standard labeling protocol provided by the manufacturer. The final concentrations of the
362 labelled proteins were the same as for thrombolytic experiments, i.e., 1.3 µg/mL. Thrombolytic
363 efficiencies of labelled plasminogen activators were verified in the static model.

364 **Penetration rate analysis**

365 Protein penetration rate through the fibrin gel was determined by continuous measurements of
366 fluorescence intensities at a distance of up to 1 mm from the front of the plasminogen activator
367 application site[31]. The penetration rate was expressed as the relative fluorescence intensity (RFI)
368 at a given distance and time. RFI was determined using a custom image analysis script in the
369 Python programming language. Penetration rate data were further normalized to relevant
370 controls. Data were expressed as mean ± standard deviation, if not otherwise indicated. The
371 generated box plots were presented as mean value (cross), median (line), interquartile range
372 (box), and minimum and maximum value (whiskers). ANOVA with post-hoc Tukey's HSD test was
373 used to compare data. P-values ≤ 0.05 were considered to be statistically significant. All analyses
374 were performed using GraphPad Prism (GraphPad Software Inc.).

375 **Preparation of clots for *in vivo* assays**

376 Details of the characteristics and nature of artificial clots are the subject of a previous project[40],
377 and their preparation is therefore described only briefly. Commercial human fibrin glue Tisseel
378 kit (Baxter) was used to generate artificial clots for *in vivo* experiments. Saline solution (1.5 mL)
379 and $BaSO_4$ suspension (0.5 mL) (Micropaque, Guerbet) were injected into the original "TISSEEL"
380 ampoule. 1 mL of the original calcium chloride solution and 5 mL of bovine serum were injected
381 into the "Thrombin 500 I.U." original ampoule. Finally, "TISSEEL" and "Thrombin 500 I.U."
382 preparations were injected in a 1:1 ratio into a PE60 and PE10 tubes (Braintree Scientific) for
383 the thrombolytic effectivity study and the safety study, respectively, using the original Duploject
384 system (Baxter). Both ends of the cannula containing clot components were hermetically sealed
385 to prevent any evaporation or desiccation, and the mixture was incubated at 37 °C for 120 min,
386 followed by storage at 4–8 °C for additional 24 hours. The resulting artificial clot was cut into

387 10 mm fragments for the effectivity study and 1 mm fragments for the safety study and the
388 corresponding samples were stored in the saline solution in an Eppendorf tube at –20 °C.

389 **Thrombolytic effectivity study *in vivo***

390 Adult male outbred Wistar rats (n=68; body weight 120–180 g) were selected for the *in vivo* lysis
391 experiments and were randomized into groups with different treatment regimens (variable
392 thrombolytic types, doses, and administration routes) as described in **Table 1**.

393 **Table 1: Overview of animal experimental groups for *in vivo* effectivity study based on different treatment**
394 **regimes.** CRI = continuous rate infusion.

Experimental group	Number of animals in the group
Control group (saline solution)	10
Alteplase (0.9 mg/kg, CRI)	16
Tenecteplase (0.25 mg/kg, bolus)	12
Brnoteplase (0.9 mg/kg, CRI)	4
Brnoteplase (0.9 mg/kg, bolus)	12
Brnoteplase (2.5 mg/kg, bolus)	12
Brnoteplase (5.0 mg/kg, bolus)	2

395

396 The exclusion criterion for the experiment was death during the anesthesia or the surgical
397 procedures before the clot delivery. Throughout the thrombolysis experiment, rats were under
398 general anesthesia induced by inhalation of 2.5 % isoflurane in filtered room air as a carrier gas.
399 After the intramuscular application of xylazine and ketamine (5 mg/kg and 35 mg/kg of body
400 weight, respectively), a mixture of urethane (80 mg/mL) and alpha-chloralose (6 mg/mL) at a
401 dose of 8 mL/kg of body weight was applied into the peritoneal cavity. Subsequently, the left
402 common carotid artery (CCA) was dissected, visualized, and cannulated in a retrograde direction
403 with a PE50 (Braintree Scientific) cannula.

404 Three individual barium-labeled artificial clots were injected via the PE50 catheter cannula into
405 the aortic arch of each tested rat. Micro-fluoroscopy using the C-arm LabScope system
406 (Glenbrook Technology, Inc.) was used to verify the localization of the introduced clots in the
407 branches of the abdominal aorta and the position of the animals was then adjusted to achieve
408 the optimal visibility of the clots with the maximum area of their size and without the shielding
409 of bone structures. The initial image was captured at time zero (before the thrombolytic drug

410 administration). Subsequently, a bolus injection/continuous rate infusion of a tested
411 thrombolytic was initiated. The continuous rate infusion treatment consisted of an initial bolus
412 of 10 % of the total dose volume, followed by an infusion of the remaining 90 % volume for 60
413 minutes. In the bolus treatment groups, the entire volume of the thrombolytic agent was
414 administered at once. The control group received an equivalent volume of intravenous saline
415 solution. The therapy was monitored for 60 minutes by the C-arm micro-fluoroscopy and
416 radiographs were acquired and stored every 5 minutes.

417 After the experiment, the animals did not regain consciousness. Euthanasia was performed by
418 overdose of anesthetics (0.7 mL of 2 % xylazine + 0.7 mL of 10 % ketamine administered
419 intraperitoneally). Due to the possibility of cross-reactions between analgesics and tested
420 thrombolytic compounds, analgesics were not used.

421 ***In vivo* thrombolytic effectivity study outcome analysis**

422 The outcome was measured as a relative area change of each monitored artificial clot, and the
423 lysis rate was then calculated as a linear fit of relative area change over time. All collected
424 radiographs were analyzed using the ImageJ 1.52a software (Wayne Rasband, National Institutes
425 of Health), and the area of identified clots in pixels was manually determined at each time point.
426 All images of one animal were measured simultaneously in one reading sequence. Two
427 independent observers performed the image analysis, blinded to one another's results and to
428 animal group assignment. Anatomical determination of arteries with clots was performed after
429 all measurements. A standardized protocol was established and followed for non-standard clot
430 positions or movements: (1) If the area of two clots in different arteries overlapped, the size was
431 measured as a single clot. (2) If the lysis of the clot caused its movement but the clot was still
432 visible on the image, the shadow area of the clot was included in the original area of the clot.
433 (3) The image was excluded if the clot moved out of the image.

434 The change in the artificial clot area (CAC) was calculated from the clot area at a calculated
435 time (a_t) relative to the clot area at time zero baseline before thrombolytics administration (a_0),
436 i.e., at the beginning of the experiment, based on **Equation 10**. The lysis rate in $\%.min^{-1}$

437 represents a relative change in the area of the artificial clot (CAC) divided by the minute in which
438 the area was measured (t) based on **Equation 11**. Results of the thrombolysis were used to
439 generate the thrombolytic curve. The area under the thrombolytic curve (AUC) was calculated
440 and used as a comparative parameter among the tested and control groups. All analyses were
441 performed using Excel for Microsoft 365 MSO version 2405 (Microsoft Corporation) and GraphPad
442 Prism version 8.0.0 (GraphPad Software Inc.).

$$CAC = \frac{a_0 - a_t}{a_0} \cdot 100\ \% \tag{10}$$

$$\text{lysis rate} = \frac{CAC}{t} \tag{11}$$

443 **Safety study**

444 The safety study was based on a thromboembolic Middle Cerebral Artery Occlusion (MCAO)
445 model, utilizing the same clot type as in the thrombolytic effectivity study. However,
446 embolization to all major cerebral arteries, namely the anterior, middle, and posterior cerebral
447 arteries, was included. This approach is referred to as the **C**ircle **o**f **W**illis **B**ranches **O**cclusi**o**n -
448 CoWBOi model. Male outbred Wistar rats, weighing between 480 and 980 grams and aged 7 to 9
449 months, were housed individually under standard conditions, with a natural light/dark cycle and
450 unrestricted access to food and water. Animals were randomly assigned to one of three
451 experimental groups, receiving either alteplase (0.9 mg/kg, continuous rate infusion, n=25,
452 included n=22), tenecteplase (0.25 mg/kg, bolus, n=25, included n=24), or Brnoteplase (2.5
453 mg/kg, bolus, n=23, included n=22). Rats, that did not develop cerebral stroke or died within
454 120 minutes of thrombolytic treatment, were excluded from the study.

455 General anesthesia was induced via inhalation of 2.5 % isoflurane, followed by intramuscular
456 administration of xylazine (5 mg/kg), ketamine (35 mg/kg), and intraperitoneal diazepam (2
457 mg/kg). Due to the possibility of cross-reactions between analgesics and tested thrombolytic
458 compounds, analgesics were not used. Embolization was performed in a modified version of the
459 standard MCAO model, with cannulation of the left external, and internal carotid arteries. Two
460 embolic clots (1.5 mm × 0.3 mm) were introduced into the intracranial internal carotid artery.

461 Thrombolytic treatment was initiated 4 hours post-embolization. After 24 hours, the animals
462 were euthanized by overdose of anesthetics (0.7 mL of 2 % xylazine + 0.7 mL of 10 % ketamine
463 administered intraperitoneally), and their brains were collected in cold saline without flushing.
464 As described previously, the extracted brains were fixed in formalin for 24 hours and stained
465 with iodine[41] . In contrast with the original set-up, the brains were not examined in agarose but
466 in paraffin oil. Micro-computed tomography (miCT) imaging was performed using a SkyScan1276
467 CMOS (Bruker) scanner, and the acquired scans were analyzed using the Amira software (Thermo
468 Scientific). Examiners were blinded to group assignments to ensure unbiased assessment.

469 ***In vivo* safety study outcome analysis**

470 To evaluate hemorrhagic transformation (HT), a classification system based on ECASS II criteria[42]
471 was applied. Hemorrhagic transformation was categorized into four subtypes (HI1, HI2, PH1, and
472 PH2) according to the criteria listed in **Table 2**. Considering that thrombolytic enzymes were
473 administered 4 hours after clot embolization, by which time all collateral vessels had already
474 closed due to ischemic damage, successful recanalization in this model was consistently
475 associated with hemorrhagic transformation.

476 **Table 2: Hemorrhagic transformation (HT) classification based on the ECAS II study**. The classification
477 recognizes four HT subtypes (HI1, HI2, PH1, and PH2) that differ in the listed criteria.

Grade	Description
HI1	Petechial hemorrhages at infarct margins
HI2	Petechial hemorrhages throughout the infarct without mass effect
PH1	Hemorrhage affecting ≤30 % of the infarcted area with minor mass effect
PH2	Hemorrhage affecting >30 % of the infarcted area with substantial mass effect

478

479 To quantify hemispheric asymmetry (HA), we calculated the affected hemisphere volume
480 (*affected*) and the intact hemisphere volume (*intact*), excluding the olfactory bulbs and
481 cerebellum from the analysis. The percentage of HA was then derived using **Equation 12**. A
482 hemispheric asymmetry of 6 % was identified as the threshold distinguishing normal from
483 pathological brains. Values exceeding this threshold were consistently associated with the
484 presence of cerebral edema.

$$HA = \frac{affected - intact}{intact} \cdot 100\ \% \quad (12)$$

485 **Quantification of residual plasminogen, plasmin, and thrombolytic levels in rat plasma**

486 At the end of the *in vivo* thrombolytic effectivity study, whole blood from the common carotid
487 was collected to a K3-EDTA tube (2.7 mL, S-Monovette, Sarstedt AG). The collected blood was
488 centrifuged for 15 min at 1,500 rpm and the resulting plasma was separated into an Eppendorf
489 tube, aliquoted, and stored at -20 °C. The collected plasma samples were tested for levels of
490 plasmin, plasminogen, and a thrombolytic enzyme using ELISA Rat Plasmin Kit (MyBioSource),
491 ELISA Rat Plasminogen Kit (MyBioSource), and ELISA Human Active tPA Kit (Molecular
492 Innovations), respectively. The determination of the concentration was performed according to
493 the protocol provided by the manufacturer with no modifications. In the case of Human tPA Kit,
494 purified solutions of alteplase and Brnoteplase (the same as administered in rats) with known
495 concentrations were used to generate individual calibration curves to prevent any discrepancies
496 caused by different sources of the administered and the calibration samples. The final plasma
497 levels were calculated from the measured absorbance values based on the constructed
498 calibration curves.

499 **Consent for animals used in experiments**

500 All procedures and animal experiments were performed in full compliance with the ARRIVE and
501 the European Community Council Directive (2010/63/EU) for Protection of Vertebrate Animals
502 Used for Experimental and other Scientific Purposes guidelines. The project was approved by the
503 Masaryk University Brno Institutional Committee for the Protection of Experimental Animals and
504 by the Committee for the Protection of Experimental Animals of the Ministry of Education Youth
505 and Sports in the Czech Republic (MEYS CZ) with the protocol number MSMT-35804 / 2019-2.

506 # Results

507 **Computational design guides multi-objective selection of thrombolytic candidates**

508 To identify variants with optimized therapeutic performance, we implemented a multi-objective
509 computational design strategy that integrates complementary engineering principles. The initial
510 pool of novel thrombolytic candidates was generated *in silico* using three independent
511 approaches: (i) rational design to modulate active-site interactions and receptor binding, (ii)
512 ancestral sequence reconstruction to access robust and evolutionarily optimized scaffolds, and
513 (iii) database mining to uncover sequence diversity supporting enhanced fibrin selectivity and
514 inhibition resistance (**Table 3**, **Figure S1**). By explicitly considering multiple catalytic and
515 biophysical properties during candidate selection, this framework prioritizes variants with
516 balanced improvements across efficiency, selectivity, functional stability, and safety, providing
517 a focused set of promising enzymes for experimental evaluation.

518 **Rational design** focused on reducing interactions with clearance and signaling receptors,
519 particularly LRP1 and NMDAR, which are implicated in short half-life and neurotoxicity. This was
520 achieved by introducing Tyr67Asn and Ser69Ala mutations shown to prevent glycosylation
521 responsible for LRP1 binding[43] (resulting in variant Alt03), and by combining these mutations with
522 additional substitutions of lysine residues (yielding variants Alt01 and Alt02). Lysine residues are
523 known to mediate LRP1 interaction. Alt01 includes additional Lys10Glu, Lys49Ile, and Lys152Gln
524 mutations which were selected using structure-based computational tools, namely protein-
525 protein docking, molecular dynamics, surface exposure analysis, and thermodynamic stability
526 predictions (**Supplementary Note 1**). Alt02 incorporates additional Lys82Ala, Lys159Ser, and
527 Lys162Ile mutations selected based on their sequence conservation in desmoteplase, which has
528 been shown to compete with alteplase for the LRP1 binding site[44] (**Supplementary Note 2**).
529 Finally, the Brnoteplase variant was constructed by combining the two original substitutions
530 preventing LRP1-binding glycosylation[43] (Tyr67Asn and Ser69Ala) with mutations decreasing PAI-
531 1 inhibition and increasing fibrin specificity[45] (Lys296Ala, His297Ala, Arg298Ala, Arg299Ala),
532 disabling NMDAR-mediated neurotoxicity[46] (Trp253Arg), and removing high-mannose
533 glycosylation responsible for the low alteplase biological half-life[47] (Asn117Gln).

534 **Ancestral sequence reconstruction (ASR)** strategy utilized the FireProt^{ASR} webserver to
535 explore evolutionary and functional diversity while preserving thrombolytic activity. The analysis
536 produced a phylogenetic tree comprising 150 extant alteplase homologs and 149 ancestral
537 sequences (**Figure S2**). Two ancestral nodes close to alteplase, named AltAnc01 and AltAnc02,
538 were selected based on sequence identity and conservation of catalytic residues (**Table 3**).
539 AltAnc01 is ancestral to alteplase and four other extant sequences annotated as plasminogen
540 activators (PAs), while AltAnc02 is ancestral to alteplase, ten additional annotated PAs, and one
541 hypothetical protein predicted to be a PA (**Supplementary Note 3**).

542 **Database mining** using the EnzymeMiner webserver identified naturally occurring homologs
543 of alteplase and desmoteplase with potentially favorable biochemical features. Over 10,000
544 mined sequences were filtered based on predicted solubility, absence of transmembrane regions,
545 and preservation of essential catalytic domains and residues, resulting in 198 alteplase and 615
546 desmoteplase homologs meeting these criteria. From these, we manually selected five
547 candidates (**Table 3**): three homologous to alteplase (AltEM01–03) and two to desmoteplase
548 (DesEM01–02). The selected sequences originate from bottlenose dolphin, Bolivian squirrel
549 monkey, Angolan colobus, and vampire bat (**Supplementary Note 4**).

550 **Table 3: Summary of *in silico* designed and selected thrombolytics for experimental testing.** Variants
551 highlighted in grey could not be experimentally produced, therefore, were not characterised. Full sequences of
552 all variants are provided in **Figure S1**. ASR = ancestral sequence reconstruction.

Variant naming	Modification strategy	Parental Protein	Sequence modification
Alt01	Rational design	Alteplase	K10E/K49I/Y67N/S69A/K152Q
Alt02	Rational design	Alteplase	Y67N/S69A/K82A/K159S/K162I
Alt03	Rational design	Alteplase	Y67N/S69A
Brnoteplase	Rational design	Alteplase	Y67N/S69A/N117Q/W253R/K296A/H297A/R298A/R299A
AltAnc01	ASR	Alteplase	76.6 % identity to alteplase; ancestral to 5 extant genes
AltAnc02	ASR	Alteplase	71.0 % identity to alteplase; ancestral to 12 extant genes
AltEM01	Database mining	Alteplase	78.4 % identity to alteplase; gene isoform X1 from bottlenose dolphin
AltEM02	Database mining	Alteplase	82.7 % identity to alteplase; gene isoform X2 from bottlenose dolphin

AltEM03	Database mining	Alteplase	92.0 % identity to alteplase; gene from Bolivian squirrel monkey
DesEM01	Database mining	Desmoteplase	68.0 % identity to alteplase; gene isoform X3 from Angolan colobus monkey
DesEM02	Database mining	Desmoteplase	80.0 % identity to alteplase; gene from white-winged vampire bat

553

554 **Biochemical profiling reveals Brnoteplase with enhanced thrombolytic properties**

555 Gene sequences encoding putative and mutant plasminogen activators selected *in silico* were
556 experimentally constructed, and 8 out of 11 selected thrombolytic proteins were successfully
557 produced recombinantly. Our comprehensive biochemical characterization (**Figure 2**, **Table S1**)
558 revealed that all the proteins exhibited clear thrombolytic activity (**Figure 2a**, **Figure S3**, **Table**
559 **S1**), validating the robustness of our computational approach for accurately predicting and
560 designing plasminogen activator enzymes. Thermal stabilities of all characterized proteins
561 (**Figure 2d**, **Figure S4**, **Table S1**) were highly above the physiological temperature, allowing their
562 administration to the human body without a risk of rapid thermal inactivation.

563 Fibrinogen and fibrin stimulation analysis (**Figure 2b**, **Figure S3**, **Table S1**) yielded
564 unimpaired profiles for Alt01–03 compared to alteplase ($p=0.37$, $p=0.35$, $p=0.49$, respectively),
565 whereas other variants showed significantly lower fibrin stimulation ($p<0.001$) and activity
566 ($p<0.001$), suggesting inefficient thrombolysis on fibrin clots. Remarkably, the variant
567 Brnoteplase displayed minimal activity with no stimulation and when stimulated by fibrinogen,
568 but it was massively stimulated by fibrin, 5.2-fold more than alteplase ($p<0.001$). This resulted
569 in an extraordinary Brnoteplase fibrin selectivity of 1020 ± 360 (**Figure 2c**, **Figure S3**, **Table S1**)
570 that was much higher than for alteplase (13.5 ± 2.0) but similar to highly selective thrombolytics
571 desmoteplase (1320 ± 220) and tenecteplase (1050 ± 170).

572 All four sufficiently fibrin-active variants, Alt01–03 and Brnoteplase, further exhibited
573 significantly increased resistance to PAI-1 inhibition ($p<0.001$) and reduced fibrin binding
574 ($p<0.001$) compared to alteplase, indicating improved potential for clot penetration and lysis
575 throughout the entire volume from inside. The highest inhibition resistance (4.2-fold higher than

576 that of alteplase) was observed for the variant Brnoteplase (**Figure 2e**, **Figures S5 and S6**, **Table**
577 **S1**), while the most pronounced reduction in fibrin binding was observed for Alt01, followed by
578 Brnoteplase (**Figure 2f**, **Figures S7 and S8**, **Table S1**) by providing 3.9- and 2.3-fold lower
579 affinities compared to that of alteplase, respectively.

580 In summary, multi-objective biochemical evaluation identified Brnoteplase as a thrombolytic
581 variant with superior functional properties compared to alteplase, combining: (i) 80-fold
582 enhanced fibrin selectivity, (ii) 4-fold increased resistance to PAI-1 inhibition, and (iii) 4-fold
583 improved penetration potential.

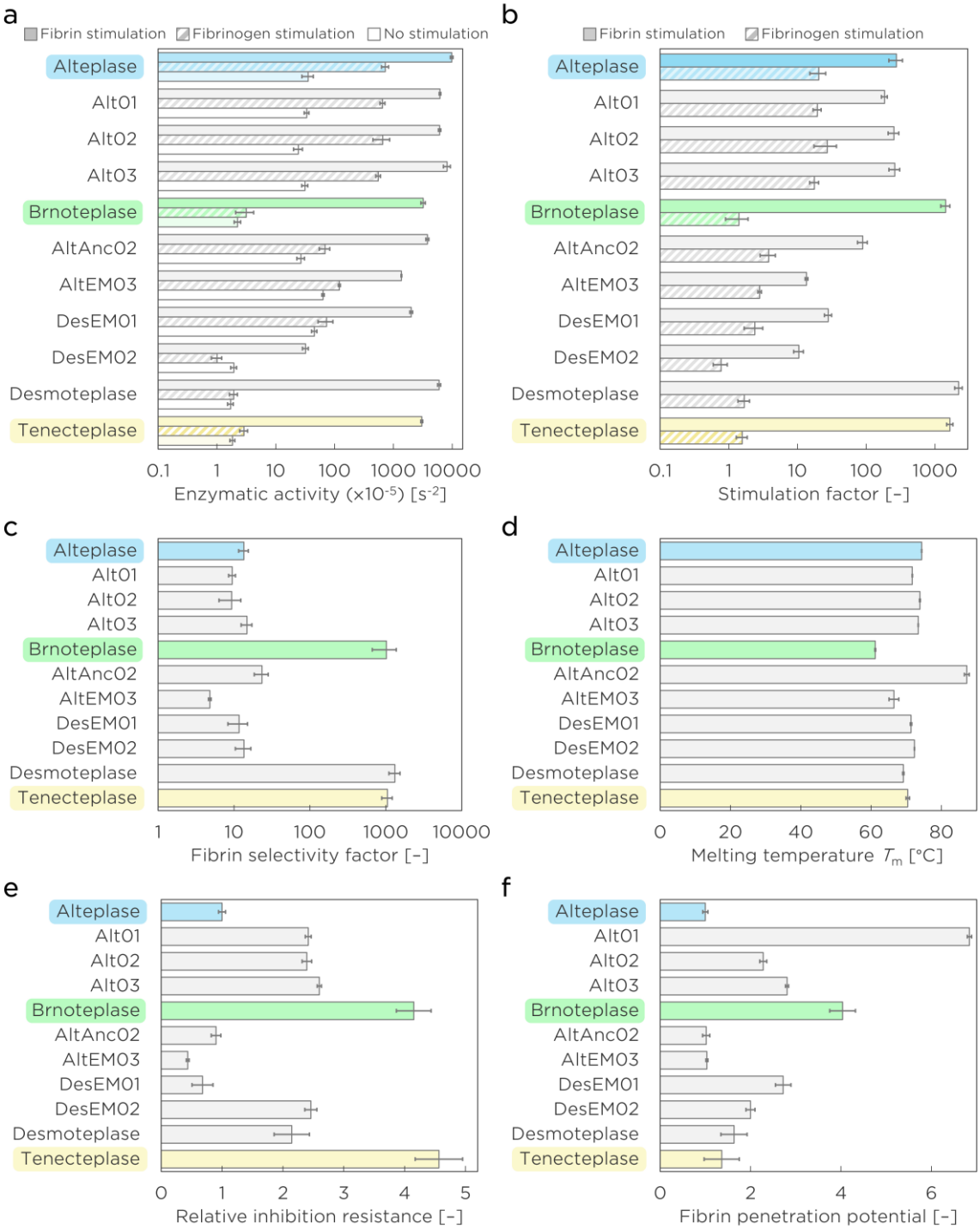

Figure 2: Biochemical characterization of thrombolytic variants. Clinically used variants alteplase and tenecteplase are highlighted in blue and yellow, respectively. The variant Brnoteplase, which was selected for further *in vitro* and *in vivo* testing, is highlighted in green. The bars represent mean values and the whiskers correspond to standard errors. For all measured data and presented values, n=3. (**a**) Comparison of plasminogen activation enzymatic activities (dark solid bars) and their values in the presence of fibrinogen (hatched bars) and fibrin (light solid bars) stimulants. (**b**) Comparison of fibrinogen (hatched bars) and fibrin (solid bars) stimulation factors. The factors are defined as fibrin(ogen)-stimulated activity over non-stimulated activity ratios. (**c**) Comparison of fibrin selectivity factors. (**d**) Comparison of melting temperatures (T_m) to define protein thermal stability. At T_m, half of the protein molecules are unfolded. (**e**) Relative comparison of inhibition resistance towards plasminogen activator inhibitor-1 (PAI-1) calculated as a ratio of the IC_{50} value for a tested protein over the IC_{50} value for alteplase (reference benchmark protein). (**f**) Relative comparison of fibrin penetration potential calculated as a ratio of the fibrin dissociation constant (K_d) value for a tested protein over the fibrin K_d value for alteplase (reference benchmark protein). Brnoteplase exhibited superior fibrin stimulation, fibrin selectivity, PAI-1 inhibition resistance, and penetration potential. Please note the logarithmic scale of the x-axis in (**a**), (**b**), and (**c**).

600 ***In vitro* thrombolysis and penetration confirm enhanced Brnoteplase properties**

601 Alt01–03 and Brnoteplase, the four variants identified as highly fibrin-active in biochemical
602 assays, were subjected to thrombolysis testing on *in vitro* prepared human clots and compared
603 to alteplase and tenecteplase (**Figure 3**). Treatment with all tested thrombolytics in the static
604 model containing semi-synthetic clots resulted in significantly greater clot mass loss ($p<0.001$)
605 and red blood cell (RBC) release ($p<0.001$) than the untreated group (**Figure 3a**, **Figure S9**, **Table**
606 **S2**). The results of lysis efficiencies were consistent with the biochemical characterization data
607 (**Figure 2a**).

608 The concentration-dependence experiment with alteplase and the most promising variant,
609 Brnoteplase (**Figure 3b**, **Table S3**), revealed notable differences between the two tested
610 proteins. Alteplase showed no significant enhancement of thrombolysis with increasing
611 concentration, as clot mass loss at 2.6, 6.5, and 13 μg/mL was comparable to the clinically
612 relevant concentration of 1.3 μg/mL ($p=0.93$, $p>0.99$, $p=0.97$, respectively) and it even
613 decreased at the highest applied concentration of 65 μg/mL ($p=0.002$). In contrast, Brnoteplase
614 exhibited a clear trend of increasing thrombolytic efficacy with increasing dosing: clot mass loss
615 was comparable to the clinically relevant concentration only at 2.6 μg/mL ($p=0.96$) while
616 significantly greater lysis was observed at 6.5, 13, and 65 μg/mL ($p=0.02$, $p<0.001$, $p<0.001$,
617 respectively). At higher concentrations of 6.5 and 13 μg/mL, Brnoteplase reached the
618 comparable level of lysis as for alteplase ($p>0.99$, $p=0.20$, respectively), and it even surpassed
619 alteplase efficiency at the highest concentration of 65 μg/mL ($p=0.009$).

620 Similar trends were observed for RBC release analysis with semi-synthetic clots (**Figure S10a**,
621 **Table S3**) and RBC-dominant clots (**Figure S10bc**, **Table S4**), confirming the validity of the
622 measured data (details in **Supplementary Note 5**). In the flow model (**Figure 3c**, **Figure S11**,
623 **Table S5**), alteplase provided lower recanalization time ($p=0.005$), greater clot reduction rate
624 ($p<0.001$), and greater RBC release ($p=0.006$) compared to the untreated group only at the
625 clinically relevant concentration (1.3 μg/mL), while higher concentrations yielded no significant
626 effect compared to the untreated group. In contrast, Brnoteplase was significantly more
627 effective than the untreated group across all tested concentrations (details in **Supplementary**

628 **Note 6**), supporting the concentration-dependent trend observed in the static model (**Figure**
629 **3b**).

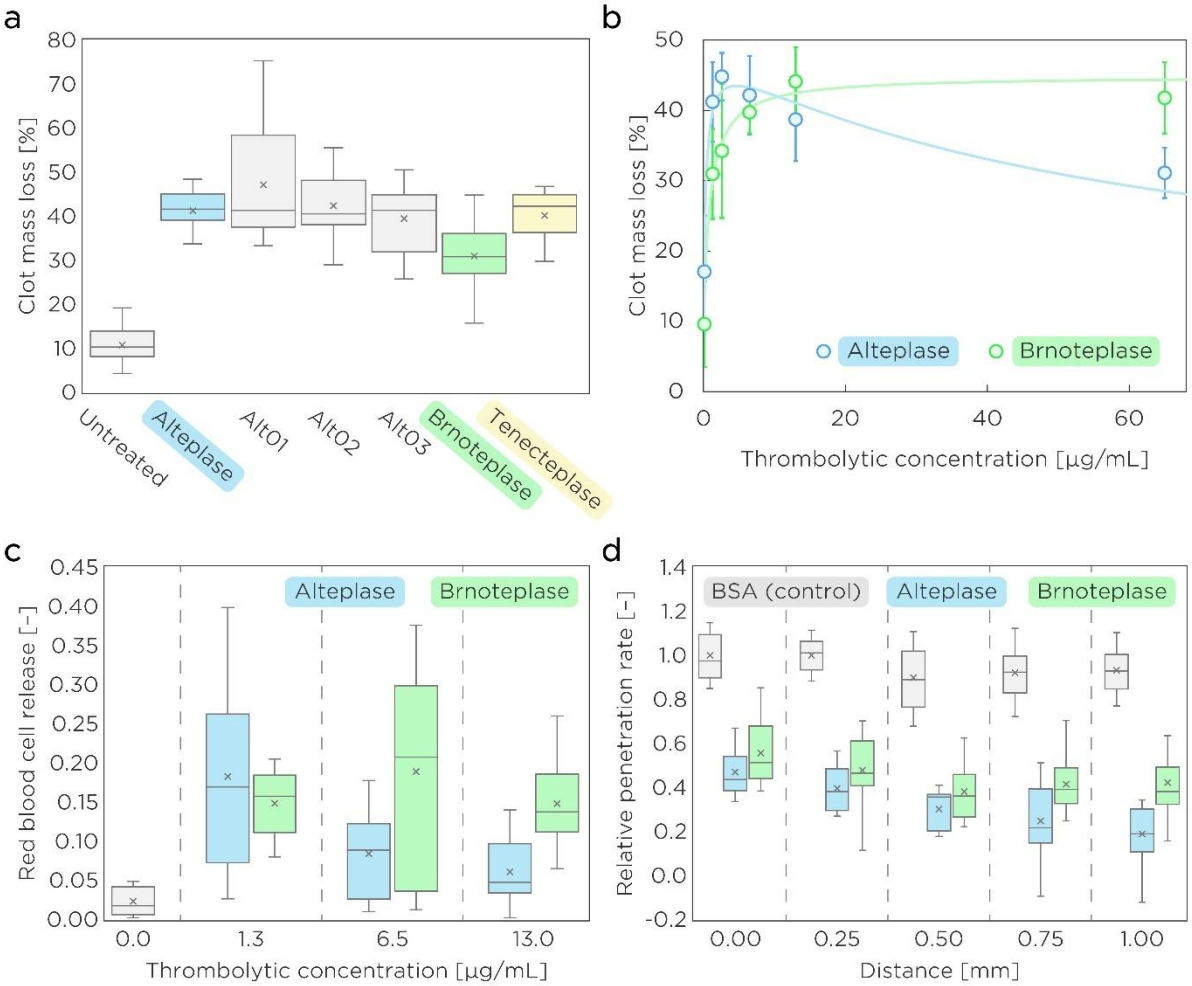

630
631 **Figure 3: *In vitro* analysis of thrombolysis efficacy and fibrin penetration.** (**a**) Comparison of thrombolytic
632 efficacy in the static model with semi-synthetic clots expressed as clot mass loss. (**b**) Concentration dependence
633 profile of thrombolytic efficacy with increasing applied concentration of a tested thrombolytic in the static
634 model. (**c**) Comparison of thrombolytic efficacy at multiple concentrations in the flow model expressed as red
635 blood cell release. (**d**) Comparison of relative penetration rates at multiple distances of a fibrin gel. Box plots
636 illustrate mean values (cross), median (line), interquartile range (box), and minimum/maximum values
637 (whiskers). Scatter plots illustrate mean values (circle) and standard errors (whiskers). The number of
638 independent experiments for each presented value are summarized in **Tables S2-S7**.

639 No significant changes in Brnoteplase thrombolytic efficacy were detected even after 3
640 months of storage at +4 °C (p=0.40), as opposed to alteplase (p=0.02), concluding the high shelf-
641 life of Brnoteplase and its suitability for long-term storage applications (**Figure S12**, **Table S6**).

642 Fibrin gel penetration experiments (**Figure 3d**, **Table S7**) confirmed detectable interaction
643 with fibrin for both alteplase and Brnoteplase, as both exhibited significant changes in
644 penetration rates (p<0.001 at all distances) compared to the non-interacting control bovine
645 serum albumin (BSA). Comparison of alteplase and Brnoteplase showed similar penetration rates

646 for both proteins up to the distance of 0.50 mm (p=0.07 at 0.00 mm; p=0.08 at 0.25 mm; p=0.06
647 at 0.50 mm). However, a significantly higher amount of Brnoteplase penetrated beyond 0.75 mm
648 (p=0.008 at 0.75 mm; p<0.001 at 1.00 mm), confirming the superior clot penetration potential
649 identified during biochemical characterization (**Figure 2f**).

650 Altogether, *in vitro* analysis confirmed the strong potential of Brnoteplase due to multiple
651 additional advantageous properties over alteplase: (i) thrombolytic efficacy increase with
652 concentration, (ii) preserved stability for over 3 months at +4 °C, and (iii) faster penetration
653 rate and greater distribution within the clot. Combined with its enhanced fibrin selectivity
654 (**Figure 2c**) and PAI-1 inhibition resistance (**Figure 2e**), the Brnoteplase profile was indicating
655 improved safety, recanalization potential, and biological half-life, which would enable bolus
656 administration and increased dosing in the subsequent *in vivo* testing.

657 **Animal testing verifies increased Brnoteplase efficiency and safety *in vivo***

658 Our selected variant Brnoteplase and approved drugs alteplase and tenecteplase were tested *in*
659 *vivo* for thrombolysis effectivity and safety in rat models (**Figure 4**). Thrombolytic effectivity
660 was assessed by the lysis rate of administered thrombi and the area under the curve (AUC) of
661 lytic curves. The Brnoteplase group (2.5 mg/kg, bolus) showed a lysis rate of 1.3 ± 0.4 %/min
662 (**Figure 4a**, **Table S8**), which was the highest among groups when compared to 0.9 ± 0.5 %/min
663 lysis rate for the alteplase (0.9 mg/kg, continuous rate infusion) and 1.1 ± 0.5 %/min for
664 the tenecteplase (0.25 mg/kg, bolus) groups. Similarly, the AUC in Brnoteplase-treated rats was
665 2350 ± 720, exceeding the values observed in the alteplase (1520 ± 810) and tenecteplase (2180
666 ± 1060) groups (**Figure 4a**, **Table S8**). Statistical analysis confirmed that Brnoteplase
667 demonstrated superior thrombolytic efficacy at all tested doses (0.9, 2.5, and 5.0 mg/kg; **Figure**
668 **S13**, **Table S8**) by providing significantly higher lysis rates and AUC values than both control and
669 alteplase (0.9 mg/kg, continuous rate infusion) groups ($p \leq 0.01$). Interestingly, Brnoteplase (0.9
670 mg/kg) demonstrated activity at the level of untreated control when applied in the continuous
671 rate infusion mode (**Table S8**).

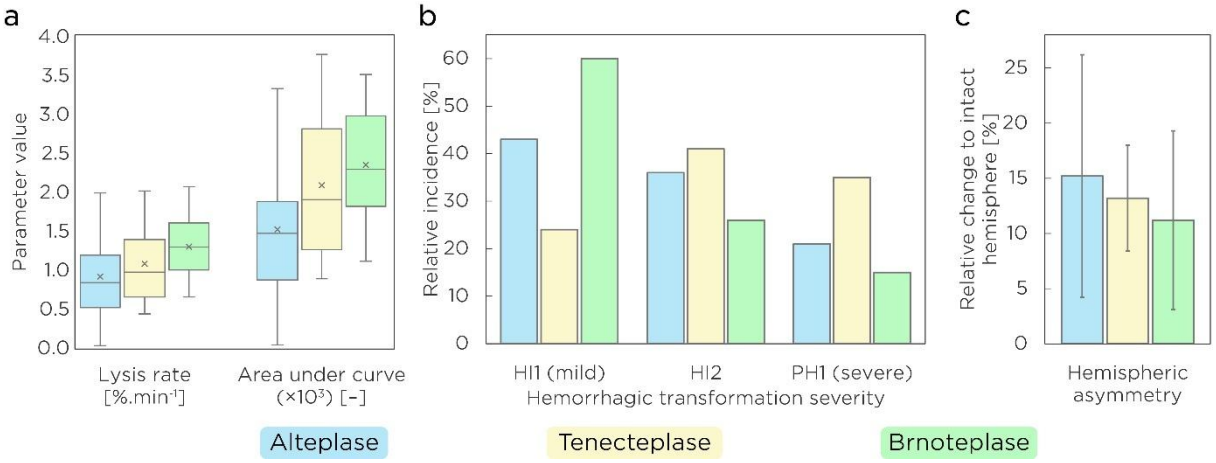

Figure 4: *In vivo* analysis of alteplase (0.9 mg/kg, continuous rate infusion), tenecteplase (0.25 mg/kg, bolus), and Brnoteplase (2.5 mg/kg, bolus) performance in animal rat models. (**a**) Comparison of the thrombolytic effectivity of alteplase (n=16), tenecteplase (n=12), and Brnoteplase (n=12), expressed as lysis rate (% of the clot dissolved per minute) and the area under the curve (AUC) of the lytic curve. Box plots illustrate mean values (cross), median (line), interquartile range (box), and minimum/maximum values (whiskers). (**b**) Proportion of hemorrhagic transformation severities according to ECASS II scoring system[42] after administering alteplase (n=22), tenecteplase (n=24), or Brnoteplase (n=22). For a detailed description, see the Methods section. (**c**) Comparison of hemispheric asymmetry of rat brains expressed as a relative change to an intact hemisphere after administering alteplase (n=22), tenecteplase (n=24), or Brnoteplase (n=22). Bar plots illustrate mean values (bars) and standard errors (whiskers).

The safety study assessed the overall incidence of hemorrhagic transformation (HT) and its severity according to ECASS II criteria[42] to evaluate the safety profile of each thrombolytic agent (**Figure 4b**, **Figure S14**, **Table S9**). Given the experimental model, in which the blood-brain barrier was damaged, and collaterals collapsed due to prolonged ischemia, bleeding could not occur without recanalization[48], making overall HT incidence an indicator of successful recanalization. HT occurred most frequently (86 %) in the Brnoteplase group (2.5 mg/kg), followed by the 71 % incidence in the tenecteplase (0.25 mg/kg), and 64 % in the alteplase (0.9 mg/kg) groups, being positively correlated with recanalization frequencies (87 %, 68 %, and 56 %, respectively; **Figure S14**, **Table S9**). Among HT subtypes, Brnoteplase treatment led predominantly to mild petechial hemorrhages (HI1), occurring in 60 % of treated rats, while only 15 % resulted in severe hemorrhages (PH1). These results substantially differed from both alteplase (43 % HI1 vs. 21 % PH1) and tenecteplase (24 % HI1 vs. 35 % PH1) groups where the proportion of severe PH1 was more prevalent (**Figure 4b**, **Table S9**).

Hemispheric asymmetry analysis (**Figure 4c**, **Table S9**) yielded the lowest value of 11 ± 8 % for Brnoteplase-treated rats (2.5 mg/kg), followed by 13 ± 5 % for tenecteplase-treated (0.25 mg/kg) and 15 ± 11 % for alteplase-treated (0.9 mg/kg) groups. The lowest asymmetry in the

699 Brnoteplase group is coupled with the highest overall HT incidence, reflecting the highest
700 recanalization frequency (**Figure S14**, **Table S9**), and the predominance of the least dangerous
701 HT grade (HI1). Together with the lowest observed proportion of severe HT (PH1; **Figure 4b**),
702 this outcome indicates that Brnoteplase treatment was associated with reduced brain swelling
703 and infarct expansion compared to the administration of alteplase or tenecteplase, suggesting a
704 potentially more favorable safety profile.

705 **Rat plasma analysis corroborates superior Brnoteplase properties**

706 Rat plasma collected at the end of the thrombolysis effectivity experiments was analyzed to
707 determine circulating levels of plasminogen, plasmin, and the administered thrombolytic (**Figure**
708 **5**, **Table S10**). Residual thrombolytic concentrations provided information about residence time
709 and half-life (**Figure 5a**, **Table S10**). The results yielded 37-, 11-, and 30-fold increased levels
710 of active Brnoteplase over alteplase at doses of 0.9, 2.5, and 5.0 mg/kg, respectively. Notably,
711 the residual active Brnoteplase concentration after administering the 0.9 mg/kg dose (0.22 ±
712 0.06 mg/L) was significantly higher even than the alteplase concentration after administering
713 5.0 mg/kg (0.09 ± 0.01 mg/L). The distinct administration regimes—bolus for Brnoteplase vs.
714 continuous rate infusion for alteplase—underscore this difference and support that the improved
715 inhibition resistance of Brnoteplase (**Figure 2e**) and potentially alleviated binding to clearance
716 receptors (**Table 3**) substantially extended its biological half-life.

717 Plasminogen and plasmin levels were quantified to evaluate the thrombolytic
718 pharmacological profile. Substantial systemic plasminemia is associated with increased
719 hemorrhagic risk, whereas preserving high plasminogen levels and restricting plasmin generation
720 to occluded areas promises more favorable treatment outcomes[17]. Accordingly, the
721 plasminogen/plasmin ratio serves as an indicator of thrombolytic selectivity and safety potential.
722 Across all tested doses (0.9, 2.5, and 5.0 mg/kg), Brnoteplase-treated rats exhibited a consistent
723 trend of higher plasminogen/plasmin ratios than the alteplase group (**Figure 5b**, **Table S10**).
724 Furthermore, Brnoteplase treatment at the dose of 5.0 mg/kg retained a comparable or even
725 higher ratio (2700 ± 130) relative to the alteplase group at the lower, clinically relevant dose of
726 0.9 mg/kg (1970 ± 510). Together with the significantly increased *in vivo* thrombolytic efficacy

727 of Brnoteplase (**Figure 4a**), these findings corroborate previously observed enhanced selectivity

728 (**Figure 2c**) and favorable safety profile (**Figure 4bc**) of Brnoteplase.

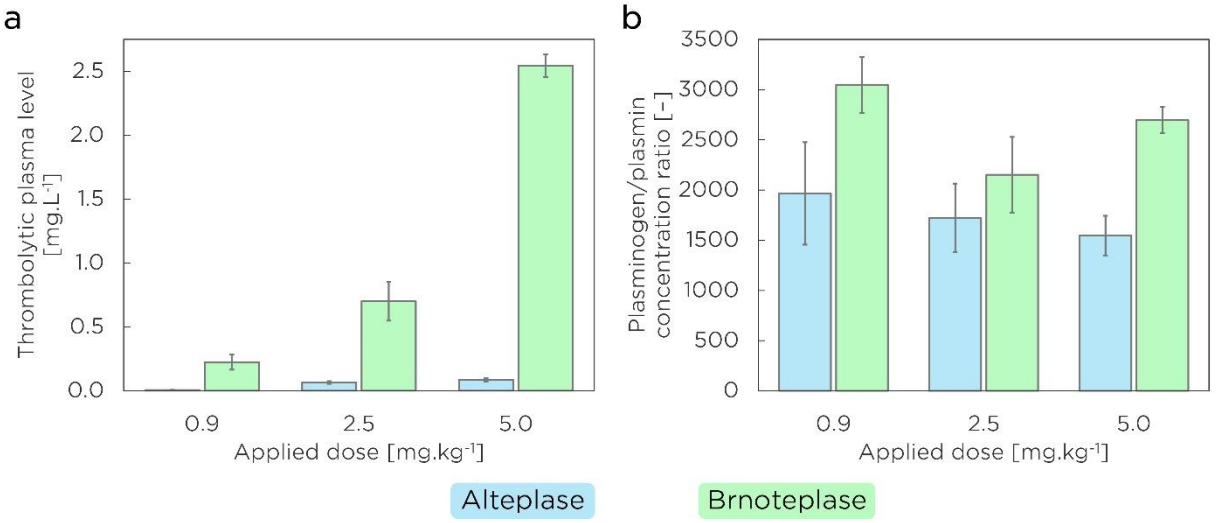

729

730 **Figure 5: Determination of pharmacological marker levels in rat plasma samples collected at the end of the**
731 **thrombolysis effectivity experiments.** The bars represent mean values and the whiskers correspond to standard
732 errors. The data were collected for alteplase applied as continuous rate infusion (n=7, 6, and 6 for the doses 0.9,
733 2.5, and 5.0 mg/kg, respectively) and Brnoteplase applied as bolus (n=16, 13, and 5 for the doses 0.9, 2.5, and
734 5.0 mg/kg, respectively). (**a**) Comparison of residual active concentrations of administered thrombolytics as an
735 indicator of the protein residence time and biological half-life. (**b**) Comparison of residual plasminogen-to-
736 plasmin ratios as an indicator of thrombolytic selectivity and safety potential.

737 # Discussion

738 In this study, we established a multi-objective enzyme engineering pipeline that integrates *in*
739 *silico* rational design, ancestral sequence reconstruction, database-guided selection, with
740 biochemical characterization, *in vitro* clot lysis and penetration assays, and *in vivo* animal
741 models. This workflow enables generation and systematic prioritization of thrombolytic
742 candidates, focusing on multiple therapeutic parameters simultaneously. Using this approach,
743 we identified Brnoteplase, a novel thrombolytic with improved pharmacological properties, and
744 it represents a promising candidate for future preclinical and clinical evaluation.

745 Biochemical characterization revealed that Brnoteplase exhibited (i) markedly enhanced
746 fibrin selectivity (80-fold higher than alteplase), (ii) superior resistance to PAI-1 inhibition (4-fold
747 higher), and (iii) increased clot penetration potential (4-fold higher). These parameters are
748 critical determinants of safer and more effective thrombolysis and provide a mechanistic basis
749 for the favorable outcomes observed in subsequent *in vitro* and *in vivo* experiments.

750 The pronounced fibrin selectivity of Brnoteplase ensures activation of plasminogen
751 predominantly within occluded regions with fibrin-containing thrombi, while minimizing systemic
752 plasminemia associated with hemorrhagic risk. As a result, Brnoteplase maintains a higher
753 plasminogen/plasmin ratio relative to alteplase *in vivo*, as confirmed by ELISA analysis of rat
754 plasma collected after thrombolysis. Additionally, the *in silico* design of Brnoteplase aimed to
755 reduce affinity for LRP1 and NMDAR which is expected to mitigate off-target central nervous
756 system interactions and thereby further enhance the safety profile[15,16]. All these findings were
757 corroborated *in vivo*, where the Brnoteplase-treated group exhibited a lower proportion of severe
758 hemorrhagic transformations compared to alteplase and tenecteplase.

759 Enhanced inhibition resistance, another major characteristic of Brnoteplase, aligns with
760 expectations from the rational design phase. This variant incorporates mutations previously
761 shown to reduce interaction with PAI-1, a primary inhibitor of tissue plasminogen activator in
762 human blood. Together with mutations designed to minimize binding to clearance receptors such
763 as LRP1 and mannose receptors, these combined features were intended to modulate protein
764 pharmacokinetics[6,49,50], and this expectation was confirmed *in vivo*. Rat plasma samples collected
765 at the end of thrombolysis experiments revealed significantly higher residual levels of active
766 Brnoteplase compared to alteplase, indicating an extended biological half-life. This enabled
767 efficient bolus administration, a clinically meaningful advantage over alteplase.

768 Finally, superior clot penetration potential of Brnoteplase in biochemical assays was derived
769 from decreased fibrin affinity. This assumption was validated by *in vitro* assays directly
770 monitoring thrombolytics motion through fibrin matrix gels. Compared to alteplase, Brnoteplase
771 exhibited a faster penetration rate and greater distribution within the clot. This facilitates lysis
772 from within the clot rather than relying solely on surface degradation, which is characteristic of
773 conventional thrombolytics. By promoting more uniform and deeper fibrinolysis, Brnoteplase may
774 accelerate recanalization, particularly in large or densely structured thrombi.

775 In addition to these mechanistic advantages, Brnoteplase demonstrated a favorable dose-
776 response profile *in vitro*. Thrombolytic efficacy progressively increased with concentration until
777 plateau, whereas alteplase exhibited an early peak with a decline at elevated doses. Combined

778 with the Brnoteplase selectivity and reduced affinity for receptors, this profile suggests that
779 higher dosing could enhance thrombolytic potency without compromising safety and hemorrhagic
780 complications. Consistent with these findings, *in vivo* experiments in rat models confirmed that
781 Brnoteplase achieved significantly higher thrombolysis rates and recanalization frequency across
782 all tested doses compared to alteplase. Importantly, safety assessments demonstrated the lowest
783 incidence of severe hemorrhagic transformation and minimal hemispheric asymmetry in
784 Brnoteplase-treated animals relative to both alteplase and tenecteplase. Nevertheless, given the
785 low overall occurrence of hemorrhagic events in the tested cohorts, larger-scale studies will be
786 required to confirm statistical significance of the safety study outcome.

787 Considering that Brnoteplase incorporates several mutations originally introduced in
788 tenecteplase, it is not unexpected that they share a similar profile in biochemical testing, namely
789 fibrin selectivity and PAI-1 resistance. However, Brnoteplase also demonstrated significantly
790 greater fibrin clot penetration and a lower rate of severe hemorrhagic transformation,
791 positioning it as a potentially advantageous alternative within the current state-of-the-art
792 thrombolytics.

793 In summary, we establish an enzyme engineering workflow that integrates multi-objective
794 design, prioritization, and multilevel functional validation for the development of improved
795 thrombolytic biocatalysts. Brnoteplase exemplifies the outcome of this approach, combining
796 enhanced fibrin selectivity, increased resistance to inhibition, prolonged functional lifetime, and
797 improved substrate accessibility within fibrin matrices. These properties collectively enhance
798 effective catalytic performance under physiologically relevant conditions, resulting in improved
799 thrombolytic activity and a favorable safety profile in preclinical *in vivo* models. Beyond the
800 specific case of Brnoteplase, our work provides a generalizable framework for optimizing
801 proteolytic enzymes operating in complex biological environments. The proposed approach builds
802 upon existing enzyme catalysis methods and emphasizes the potential of combining rational and
803 evolutionary design to create next-generation therapeutics biocatalysts., where effective
804 catalysis requires coordinated optimization of multiple parameters. While further validation in
805 advanced models is required, the presented approach expands current strategies in enzyme

806 catalysis and highlights the potential of integrating rational and evolutionary design to develop
807 next-generation therapeutic biocatalysts.

808 Funding

809 This work was supported by the Czech Ministry of Education (INBIO -
810 CZ.02.1.01/0.0/0.0/16_026/0008451, ENOCH - CZ.02.1.01/0.0/0.0/16_019/0000868); Grant
811 Agency of Czech Republic (20-15915Y and 25-18233M); and National Institute for Neurology
812 Research (LX22NPO5107 MEYS) Financed by European Union – Next Generation EU. MT, ST, and
813 JSM are supported by the scholarship Brno Ph.D. Talent and MM is supported by the Masaryk
814 University (MUNI/H/1561/2018). ST, MP, and JV received additional support from the Ministry of
815 Health of the Czech Republic in cooperation with the Czech Health Research Council under
816 project No. NW24-08-00064. Computational resources were provided by the e-INFRA CZ project
817 (ID:90254), supported by the Ministry of Education, Youth and Sports of the Czech Republic, and
818 by the ELIXIR-CZ project (ID:90255), part of the international ELIXIR infrastructure.

819 Author Contribution Statement

820 **J.M and D.B.** performed the *in silico* analysis and selection of the initial thrombolytic pool.
821 **Pe.Ka. and T.B.** produced the designed thrombolytic enzymes. **M.T. and V.S.** performed the
822 biochemical characterization of selected proteins and ELISA measurements of rat plasma samples
823 and analyzed the corresponding data. **S.T., M.P., Pa.Ki., and J.V.** performed the *in vitro*
824 thrombolysis and fibrin penetration assays and analyzed the corresponding data. **P.S., J.H., E.B.,**
825 **A.D.A., J.B., M.K., and J.O.** performed the *in vivo* animal testing and the corresponding data
826 analysis and statistical evaluation. **M.T., V.S.** drafted the initial version of the manuscript with
827 the help of **J.M., S.T., and J. V.**. **J.D., Z.P., D.B., M.M., J.V., L.K., and R.M.** conceived and
828 designed the study, supervised the project, and acquired funding. **All authors** reviewed and
829 interpreted the data, critically revised the manuscript, and approved the final version.

830

Acknowledgements

We thank the laboratory technicians Marketa Stuchla, Veronika Novakova, Irena Halikova, and Klara Markova for their assistance with the preparation of common reagents and sample storage.

Declaration of Interests

The authors declare no competing interests.

References

1. Feigin VL, Brainin M, Norrving B, et al. World Stroke Organization: Global stroke fact sheet 2025. *Int J Stroke*. 2025;20(2):132-144. doi:10.1177/17474930241308142

2. Aguiar de Sousa D, von Martial R, Abilleira S, et al. Access to and delivery of acute ischaemic stroke treatments: A survey of national scientific societies and stroke experts in 44 European countries. *Eur Stroke J*. 2019;4(1):13-28. doi:10.1177/2396987318786023

3. Xiong Y, Wakhloo AK, Fisher M. Advances in acute ischemic stroke therapy. *Circ Res*. 2022;130(8):1230-1251. doi:10.1161/CIRCRESAHA.121.319948

4. Yaghi S, Willey JZ, Cucchiara B, et al. Treatment and outcome of hemorrhagic transformation after intravenous alteplase in acute ischemic stroke: A scientific statement for healthcare professionals from the American Heart Association/American Stroke Association. *Stroke*. 2017;48(12):e343-e361. doi:10.1161/STR.0000000000000152

5. Mosconi MG, Paciaroni M. Treatments in ischemic stroke: Current and future. *Eur Neurol*. 2022;85(5):349-366. doi:10.1159/000525822

6. Mican J, Toul M, Bednar D, Damborsky J. Structural biology and protein engineering of thrombolytics. *Comput Struct Biotechnol J*. 2019;17:917-938. doi:10.1016/j.csbj.2019.06.023

7. Potla N, Ganti L. Tenecteplase vs alteplase for acute ischemic stroke: A systematic review. *Int J Emerg Med*. 2022;15(1):1. doi:10.1186/s12245-021-00399-w

8. Burwell JM, Howay JR, Wasko L, et al. Tenecteplase is here: Navigating the shift of a stroke thrombolytic in the United States prior to FDA approval: A mini-review on rationale, barriers, and pathways. *Front Neurol*. 2025;16:1563423. doi:10.3389/fneur.2025.1563423

9. Rodriguez M, Sidebottom C, Wells DA, et al. A systematic review of the efficacy and safety of tenecteplase versus alteplase in acute ischemic stroke: A time to pass the torch. *Stroke Vasc Interv Neurol*. 2024;4(4):e001110. doi:10.1161/SVIN.123.001110

10. Ma Y, Xiang H, Busse JW, et al. Tenecteplase versus alteplase for acute ischemic stroke: A systematic review and meta-analysis of randomized and non-randomized studies. *J Neurol*. 2024;271(5):2309-2323. doi:10.1007/s00415-024-12243-1

11. Rose D, Cavalier A, Kam W, et al. Complications of intravenous tenecteplase versus alteplase for the treatment of acute ischemic stroke: A systematic review and meta-analysis. *Stroke*. 2023;54(5):1192-1204. doi:10.1161/STROKEAHA.122.042335

867 12. Warach SJ, Dula AN, Milling TJ. Tenecteplase thrombolysis for acute ischemic stroke. *Stroke*.
868 2020;51(11):3440-3451. doi:10.1161/STROKEAHA.120.029749

869 13. Meng X, Li S, Dai H, et al. Tenecteplase vs alteplase for patients with acute ischemic stroke:
870 The ORIGINAL randomized clinical trial. *JAMA*. 2024;332(17):1437-1445.
871 doi:10.1001/jama.2024.14721

872 14. Van de Werf FJ. The ideal fibrinolytic: Can drug design improve clinical results? *Eur Heart J*.
873 1999;20(20):1452-1458. doi:10.1053/euhj.1999.1659

874 15. Maier W, Bednorz M, Meister S, et al. LRP1 is critical for the surface distribution and
875 internalization of the NR2B NMDA receptor subtype. *Mol Neurodegener*. 2013;8(1):25.
876 doi:10.1186/1750-1326-8-25

877 16. Baron A, Montagne A, Cassé F, et al. NR2D-containing NMDA receptors mediate tissue
878 plasminogen activator-promoted neuronal excitotoxicity. *Cell Death Differ*. 2010;17(5):860-
879 871. doi:10.1038/cdd.2009.172

880 17. Nikitin D, Choi S, Mican J, et al. Development and testing of thrombolytics in stroke. *J Stroke*.
881 2021;23(1):12-36. doi:10.5853/jos.2020.03349

882 18. Sumbalova L, Stourac J, Martinek T, Bednar D, Damborsky J. HotSpot Wizard 3.0: Web server
883 for automated design of mutations and smart libraries based on sequence input information.
884 *Nucleic Acids Res*. 2018;46(W1):W356-W362. doi:10.1093/nar/gky417

885 19. Alford RF, Leaver-Fay A, Jeliazkov JR, et al. The Rosetta all-atom energy function for
886 macromolecular modeling and design. *J Chem Theory Comput*. 2017;13(6):3031-3048.
887 doi:10.1021/acs.jctc.7b00125

888 20. Prasad JM, Young PA, Strickland DK. High-affinity binding of the receptor-associated protein
889 D1D2 domains with the low-density lipoprotein receptor-related protein (LRP1) involves
890 bivalent complex formation: Critical roles of lysines 60 and 191. *J Biol Chem*.
891 2016;291(35):18430-18439. doi:10.1074/jbc.M116.744904

892 21. Freeman R, Niego B, R. Croucher D, Pedersen LO, Medcalf RL. t-PA, but not desmoteplase,
893 induces plasmin-dependent opening of a blood-brain barrier model under normoxic and
894 ischaemic conditions. *Brain Res*. 2014;1565:63-73. doi:10.1016/j.brainres.2014.03.027

895 22. Musil M, Khan RT, Beier A, et al. FireProt^{ASR}: A web server for fully automated ancestral
896 sequence reconstruction. *Brief Bioinform*. 2021;22(4):bbaa337. doi:10.1093/bib/bbaa337

897 23. Hon J, Borko S, Stourac J, et al. EnzymeMiner: Automated mining of soluble enzymes with
898 diverse structures, catalytic properties and stabilities. *Nucleic Acids Res*. 2020;48(W1):W104-
899 W109. doi:10.1093/nar/gkaa372

900 24. Toul M, Strunga A, Damborsky J, Prokop Z. Thrombolytic proteins profiling: High-throughput
901 activity, selectivity, and resistance assays. *FEBS Open Bio*. doi:10.1002/2211-5463.70132

902 25. Toschi L, Bringmann P, Petri T, Donner P, Schleuning WD. Fibrin selectivity of the isolated
903 protease domains of tissue-type and vampire bat salivary gland plasminogen activators. *Eur*
904 *J Biochem*. 1998;252(1):108-112. doi:10.1046/j.1432-1327.1998.2520108.x

905 26. Harpaz D, Chen X, Francis CW, Marder VJ, Meltzer RS. Ultrasound enhancement of
906 thrombolysis and reperfusion *in vitro*. *J Am Coll Cardiol*. 1993;21(6):1507-1511.
907 doi:10.1016/0735-1097(93)90331-T

27. Prasad S, Kashyap RS, Deopujari JY, Purohit HJ, Taori GM, Daginawala HF. Development of an *in vitro* model to study clot lysis activity of thrombolytic drugs. *Thromb J*. 2006;4:14. doi:10.1186/1477-9560-4-14

28. Thalerová S, Pešková M, Kittová P, et al. Effect of apixaban pretreatment on alteplase-induced thrombolysis: An *in vitro* study. *Front Pharmacol*. 2021;12:740930. doi:10.3389/fphar.2021.740930

29. Víteček J, Wünschová AV, Thalerová S, et al. Factors influencing the efficacy of recombinant tissue plasminogen activator: Implications for ischemic stroke treatment. *PLOS ONE*. 2024;19(6):e0302269. doi:10.1371/journal.pone.0302269

30. Thalerová S, Wünschová AV, Kittová P, et al. A collateral circulation in ischemic stroke accelerates recanalization due to lower clot compaction. *PLOS ONE*. 2024;19(11):e0314079. doi:10.1371/journal.pone.0314079

31. Nikitin D, Mican J, Toul M, et al. Computer-aided engineering of staphylokinase toward enhanced affinity and selectivity for plasmin. *Comput Struct Biotechnol J*. 2022;20:1366-1377. doi:10.1016/j.csbj.2022.03.004

32. Diamond SL. Engineering design of optimal strategies for blood clot dissolution. *Annu Rev Biomed Eng*. 1999;1:427-461. doi:10.1146/annurev.bioeng.1.1.427

33. Acheampong P, and Ford GA. Pharmacokinetics of alteplase in the treatment of ischaemic stroke. *Expert Opin Drug Metab Toxicol*. 2012;8(2):271-281. doi:10.1517/17425255.2012.652615

34. Elnager A, Abdullah WZ, Hassan R, et al. *In vitro* whole blood clot lysis for fibrinolytic activity study using D-dimer and confocal microscopy. *Adv Hematol*. 2014;2014:814684. doi:10.1155/2014/814684

35. Rottenberger Z, Komorowicz E, Szabó L, et al. Lytic and mechanical stability of clots composed of fibrin and blood vessel wall components. *J Thromb Haemost*. 2013;11(3):529-538. doi:10.1111/jth.12112

36. Marcos-Contreras OA, Ganguly K, Yamamoto A, et al. Clot penetration and retention by plasminogen activators promote fibrinolysis. *Biochem Pharmacol*. 2013;85(2):216-222. doi:10.1016/j.bcp.2012.10.011

37. Longstaff C. Measuring fibrinolysis: From research to routine diagnostic assays. *J Thromb Haemost*. 2018;16(4):652-662. doi:10.1111/jth.13957

38. Longstaff C, Varjú I, Sótonyi P, et al. Mechanical stability and fibrinolytic resistance of clots containing fibrin, DNA, and histones. *J Biol Chem*. 2013;288(10):6946-6956. doi:10.1074/jbc.M112.404301

39. Morrow GB, Whyte CS, Mutch NJ. Functional plasminogen activator inhibitor 1 is retained on the activated platelet membrane following platelet activation. *Haematologica*. 2019;105(12):2824-2833. doi:10.3324/haematol.2019.230367

40. Vítečková Wünschová A, Novobilský A, Hložková J, et al. Thrombus imaging using 3D printed middle cerebral artery model and preclinical imaging techniques: Application to thrombus targeting and thrombolytic studies. *Pharmaceutics*. 2020;12(12):1207. doi:10.3390/pharmaceutics12121207

949 41. Kavkova M, Zikmund T, Kala A, et al. Contrast enhanced X-ray computed tomography imaging
950 of amyloid plaques in Alzheimer disease rat model on lab based micro CT system. *Sci Rep*.
951 2021;11(1):5999. doi:10.1038/s41598-021-84579-x

952 42. Hacke W, Kaste M, Fieschi C, et al. Randomised double-blind placebo-controlled trial of
953 thrombolytic therapy with intravenous alteplase in acute ischaemic stroke (ECASS II). *The*
954 *Lancet*. 1998;352(9136):1245-1251. doi:10.1016/S0140-6736(98)08020-9

955 43. Bassel-Duby R, Jiang NY, Bittick T, et al. Tyrosine 67 in the epidermal growth factor-like
956 domain of tissue-type plasminogen activator is important for clearance by a specific hepatic
957 receptor. *J Biol Chem*. 1992;267(14):9668-9677.

958 44. López-Atalaya JP, Roussel BD, Ali C, et al. Recombinant *Desmodus rotundus* salivary
959 plasminogen activator crosses the blood-brain barrier through a low-density lipoprotein
960 receptor-related protein-dependent mechanism without exerting neurotoxic effects. *Stroke*.
961 2007;38(3):1036-1043. doi:10.1161/01.STR.0000258100.04923.84

962 45. Keyt BA, Paoni NF, Refino CJ, et al. A faster-acting and more potent form of tissue
963 plasminogen activator. *Proc Natl Acad Sci U S A*. 1994;91(9):3670-3674.
964 doi:10.1073/pnas.91.9.3670

965 46. Goulay R, Naveau M, Gaberel T, Vivien D, Parcq J. Optimized tPA: A non-neurotoxic
966 fibrinolytic agent for the drainage of intracerebral hemorrhages. *J Cereb Blood Flow Metab*.
967 2018;38(7):1180-1189. doi:10.1177/0271678X17719180

968 47. Narita M, Bu G, Herz J, Schwartz AL. Two receptor systems are involved in the plasma
969 clearance of tissue-type plasminogen activator (t-PA) *in vivo*. *J Clin Invest*. 1995;96(2):1164-
970 1168. doi:10.1172/JCI118105

971 48. Ma J, Ma Y, Shuaib A, Winship IR. Improved collateral flow and reduced damage after remote
972 ischemic perconditioning during distal middle cerebral artery occlusion in aged rats. *Sci Rep*.
973 2020;10(1):12392. doi:10.1038/s41598-020-69122-8

974 49. Biessen EAL, van Teijlingen M, Vietsch H, et al. Antagonists of the mannose receptor and the
975 LDL receptor–related protein dramatically delay the clearance of tissue plasminogen
976 activator. *Circulation*. 1997;95(1):46-52. doi:10.1161/01.CIR.95.1.46

977 50. Chandler WL, Alessi MC, Aillaud MF, Henderson P, Vague P, Juhan-Vague I. Clearance of
978 tissue plasminogen activator (TPA) and TPA/plasminogen activator inhibitor type 1 (PAI-1)
979 complex. *Circulation*. 1997;96(3):761-768. doi:10.1161/01.CIR.96.3.761

980